

# Multi-Step Visual Reasoning with Visual Tokens Scaling and Verification

Tianyi Bai<sup>1,3\*</sup>, Zengjie Hu<sup>2\*</sup>, Fupeng Sun<sup>4\*</sup>, Qiu Jiantao<sup>3‡</sup>, Yizhen Jiang<sup>2</sup>,  
Guangxin He<sup>1</sup>, Bohan Zeng<sup>2</sup>, Conghui He<sup>3†</sup>, Binhang Yuan<sup>1†</sup>, Wentao Zhang<sup>2†</sup>

<sup>1</sup>HKUST, <sup>2</sup>Peking University, <sup>3</sup>Shanghai AI Lab, <sup>4</sup>Imperial College London

\* Equal contribution. ‡ Project leader. † Corresponding authors.  
wentao.zhang@pku.edu.cn, biyuan@ust.hk, {qiujiatao, heconghui}@pjlab.org.cn

June 13, 2025

## Abstract

Multi-modal large language models (MLLMs) have achieved remarkable capabilities by integrating visual perception with language understanding, enabling applications such as image-grounded dialogue, visual question answering, and scientific analysis. However, most MLLMs adopt a static inference paradigm, encoding the entire image into fixed visual tokens upfront, which limits their ability to iteratively refine understanding or adapt to context during inference. This contrasts sharply with human perception, which is dynamic, selective, and feedback-driven. In this work, we introduce a novel framework for inference-time visual token scaling that enables MLLMs to perform iterative, verifier-guided reasoning over visual content. We formulate the problem as a Markov Decision Process, involving a reasoner that proposes visual actions and a verifier—trained via multi-step Direct Preference Optimization (DPO)—that evaluates these actions and determines when reasoning should terminate. To support this, we present a new dataset, VTS, comprising supervised reasoning trajectories (VTS-SFT) and preference-labeled reasoning comparisons (VTS-DPO). Our method significantly outperforms existing approaches across diverse visual reasoning benchmarks, offering not only improved accuracy but also more interpretable and grounded reasoning processes. These results demonstrate the promise of dynamic inference mechanisms for enabling fine-grained, context-aware visual reasoning in next-generation MLLMs. Code and data are publicly released at <https://github.com/Open-DataFlow/vts-v>.

## 1 Introduction

Multi-modal large language models (MLLMs) that can perceive and reason over visual content are a foundational component of modern AI systems. By extending large language models (LLMs) with visual perception capabilities, MLLMs support a wide range of applications—from image-grounded dialogue and visual question answering to robotics and scientific analysis. Yet despite their impressive generalization, one fundamental challenge remains unsolved: *how can we conduct effective inference-time scaling for MLLMs to enable fine-grained, context-aware interaction with visual information?*

Current MLLMs typically adopt a *static inference paradigm*—processing the whole image into a static fixed set of visual tokens in a single step, and conducting all reasoning based solely on this static embedding. This approach limits the model’s ability to recover from ambiguity, occlusion, or missing detail: once the initial representation is formed, there is no mechanism to query the image again or refine visual understanding. In contrast, *human*

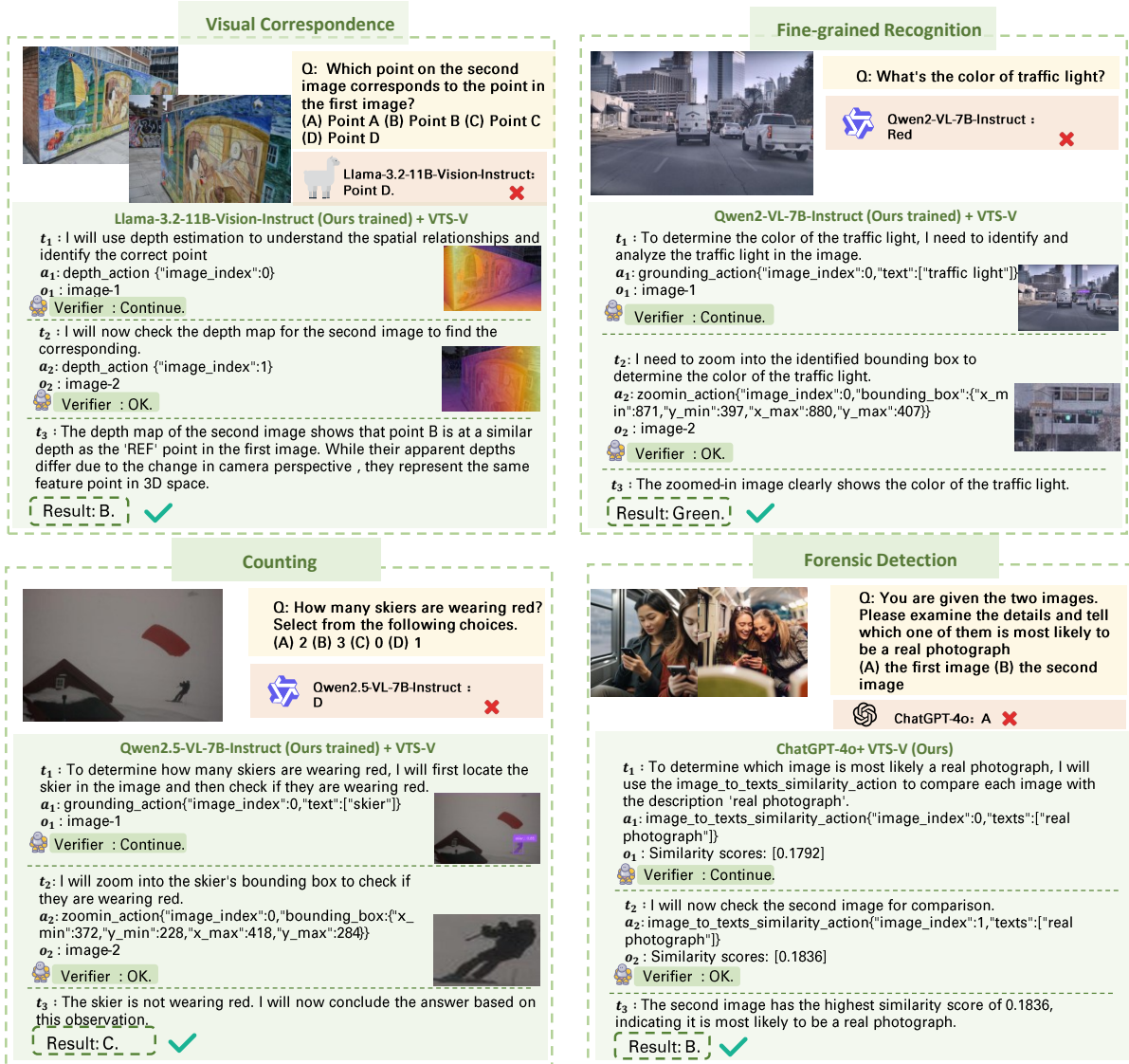


Figure 1: **Iterative Visual Reasoning with VTS-V.** Our framework equips both open-source and closed-source models with dynamic visual token scaling and step-wise verification to solve complex visual tasks. The example shows how VTS-V: (1) decomposes questions into executable steps, (2) invokes vision tools, and (3) iteratively refines answers via verifier feedback, achieving correct results. In contrast, vanilla models fail to ground detailed visual operations without token scaling, leading to incorrect answers.

*perception is inherently dynamic*—we iteratively inspect regions, zoom in, and seek new visual evidence as reasoning unfolds. Bridging this gap between static MLLM inference and dynamic human reasoning is the central problem addressed in this work.

Multi-step visual reasoning is critical for robust AI systems. Many tasks require identifying small objects, interpreting text in images, or reasoning about spatial relations—activities that benefit from an iterative, context-sensitive exploration of visual content. Furthermore, dynamic scaling enables more efficient reasoning

by focusing computational resources on the most relevant parts of the image, rather than uniformly processing all pixels or tokens. Without this flexibility, existing models exhibit degraded performance on benchmarks such as BLINK [1], V-Star Bench [2], and MMVP [3], which are designed to probe deeper visual understanding.

The core technical challenge lies in the absence of an expressive framework for flexible, inference-time visual exploration. Existing approaches either construct improved visual reasoning datasets for fine-tuning [4, 5], which still rely heavily on the pretrained model’s image-text alignment quality, or attempt to enhance inference through text token scaling [6] and the use of external vision tools [7, 8, 9, 2]. However, these methods are limited in scope, focusing narrowly on static token expansion or employing a small set of fixed visual tools in predefined pipelines. As a result, these methods fail to give the model agency in choosing what to observe next, how to focus visual attention, or when to stop reasoning. What’s needed is a unified framework that allows the model to take structured, interpretable visual actions—guided by feedback—while remaining grounded in the image content.

**Contributions.** To address this, we propose a novel framework for inference-time visual token scaling, enabling MLLMs to engage in *iterative, verifier-guided reasoning* over images. Our contributions are threefold:

- **Expressive and theoretically grounded framework.** We formulate visual reasoning as a Markov Decision Process (MDP) with two key components: a *reasoner* that proposes visual actions, and a *verifier*, trained via multi-step Direct Preference Optimization (DPO), which evaluates action quality and terminates reasoning when appropriate. We prove that our reasoner and verifier cooperation system ensures alignment between reasoning actions and visual content, while guaranteeing a bounded number of steps through an early stopping mechanism.
- **A new dataset for tool-augmented visual reasoning.** We introduce a two-part dataset: *VTS-SFT* (supervised reasoning trajectories with tool use), and *VTS-DPO* (preference-labeled reasoning pairs). These resources enable effective training of both the reasoner and verifier, supporting dynamic visual interaction with multi-step grounding.
- **Comprehensive evaluation and state-of-the-art results.** Our experiments span a variety of vision-language tasks demanding multi-step reasoning. Across these scenarios, our approach significantly outperforms strong baselines, including models augmented with limited tool use and those employing chain-of-thought prompting. We observe not only accuracy improvements but also more interpretable reasoning traces, as the model’s step-by-step process explicitly justifies each answer with visual evidence. These results underscore the effectiveness of inference-time visual token scaling: by enabling an AI to look deeper into images in a controlled, stepwise fashion, we achieve new state-of-the-art performance on tasks that previously stymied conventional MLLMs.

These contributions move us toward flexible, grounded, and interpretable visual reasoning in MLLMs—crucial for building AI systems that can “think with their eyes.”

## 2 Related Work

**Visual reasoning.** Visual reasoning in VLMs focuses on integrating visual and textual inputs to enable effective decision-making. Early approaches, such as Shikra [6], applied Chain of Thought (CoT)[10] techniques to visual tasks. Meanwhile, methods like SoM[11] and Scaffolding [12] improved reasoning by leveraging visual anchors, such as segmentation maps. V\* [2] introduced a two-step CoT approach for high-resolution visual search, demonstrating the potential of structured reasoning in visual contexts. More recently, efforts have been made to develop improved reasoning datasets for training visual language models (VLMs) [5, 4]. However, most of this work primarily focuses on scaling text tokens during the visual reasoning phase. Limited attention has been given to frameworks that scale visual tokens to address complex visual reasoning tasks.

**Visual programming and tool-using.** Recent research has focused on integrating visual tools with large language models (LLMs) and vision-language models (VLMs) to address complex visual tasks. These studies aim to leverage LLMs and VLMs to generate code that utilizes external vision tools for solving complex vision problems [7, 8, 9, 13]. For instance, Visprog [8] and ViperGPT [9] prompt VLMs to produce single-step

Python code that interacts with external vision tools, while Visual Sketchpad [7] enhances these methods by introducing multi-step reasoning capabilities, enabling VLMs to rethink and correct execution errors. However, these approaches fail to address the critical aspect of iterative visual reasoning, as their reasoning steps are typically limited to only 1–2 steps. This prevents them from performing reflective refinements akin to VLMs, hindering their ability to tackle complex visual tasks that require deeper inference and multi-step adjustments.

**Verifier design.** Recent advancements have leveraged verifiers to enhance language model reasoning and solution quality. Approaches include deriving reward signals for reasoning [14, 15], combining solution- and step-level verifiers for math problems [16], and using graph search or Monte Carlo rollouts for rationale generation [17, 18]. Training methods range from human annotations for RL with feedback [19] to synthetic data for RL with AI feedback [20]. Some treat verifiers as generative models, scoring solutions via control tokens [21] or likelihoods [22]. Closely related is V-STaR [23], which uses Direct Preference Optimization (DPO) for solution ranking. However, existing verifiers are typically designed for specific tasks and tailored training datasets. Our work utilizes multi-step DPO as a verification mechanism, supported by theoretical guarantees.

### 3 Visual Tokens Scaling with Verification

We first formally formulate the visual reasoning tasks with visual token scaling and verification.

#### 3.1 Problem Formulation

At the first step, a question-image pair  $s_1$ <sup>1</sup> is sampled from some distribution  $\mathcal{D}$  as the initial state. For each step  $h \geq 2$ , we conduct:

- **Planning:** the VLM observes the current state  $s_h$ , which is the history of the previous  $h-1$  reasoning steps, i.e.,  $s_h = (s_{h-1}, t_{h-1}, a_{h-1}, o_{h-1})$ , and generates planning of  $h$ -th step  $t_h$  by some distribution  $p(\cdot | s_h)$ .  $t_h$  can be regarded as the text tokens and determines how to manipulate the image at the  $h$ -th step.
- **Action:** based on planning  $t_h$ , the VLM further chooses an action  $a_h \in \mathcal{A}$  according to policy  $\pi(\cdot | t_h)$ , where  $\mathcal{A}$  is the finite action (module) set. This means that the VLM decides which visual module to implement for a specific instruction  $t_h$ .
- **Observation:** in response to the action, the environment then returns a visual observation  $o_h = f_{a_h}(t_h)$  for some deterministic function  $f$ . Here the visual observation is assumed to be deterministic since it is the code execution result by some visual module, the depth map of an image, for example.

Then we transit to a new state  $s_{h+1}$  and a new reasoning step begins.

- **Verification:** after each set of planning, action and observation, a verifier  $r^*$  is designed to decide whether to continue this iterative reasoning, or to stop and give out the final result.

We regard the final planning as the final result of the initial question-image pair. Eventually, we will collect a reasoning sequence

$$\tau = (s_1, t_1, a_1, o_1, \dots, t_{H_\tau}, a_{H_\tau}, o_{H_\tau}, t_{H_\tau+1}) = s_{H_\tau+1} \cup \{t_{H_\tau+1}\}, \quad (1)$$

where  $H_\tau$  (a random variable) is the length of the total reasoning steps for path  $\tau$ .

#### 3.2 Visual Reasoning with Visual Token Scaling and Verification

To enhance performance in visual reasoning tasks, the reasoning process will consist of two main components: a reasoner capable of generating visual reasoning steps, and a verifier that guides the reasoner in visual token scaling and determines the terminal condition.

**Reasoner.** The reasoner is a pre-trained VLM augmented with plug-and-play modules, which are denoted by  $R_{\theta_0}$ , where  $\theta_0$  encapsulates all the parameters. The module tools can be off-the-shelf vision models (depth maps,

<sup>1</sup>In practice,  $s_1$  will also include system prompts.

bounding box generation, etc), table operations (add columns, select row, etc), web search engines, and Python functions (plot figures, calculation, etc). The reasoner is supposed to present the reasoning steps in a sequential format as in equation (1), where  $p(\cdot | s_h) = \mathbb{R}_{\theta_0}(\cdot | s_h)$  and  $\pi(\cdot | t_h) = \mathbb{R}_{\theta_0}(\cdot | t_h)$ . In practice, the reasoner can be: (i) a model such as GPT-4o; or (ii) an open-source model fine-tuned on self-crafted datasets. In this case,  $\theta_0$  can be further updated to  $\hat{\theta}_{\text{SFT}}$  by SFT.

**Verifier.** The verifier  $r^*$  is a function that maps the reasoning trajectory generated by the reasoner to a real number. At each reasoning step  $h$ , the reasoner will continue to generate one additional step if the reward difference between step  $h$  and step  $h+1$  is no less than some predetermined positive threshold  $\epsilon$ . In this paper, we utilize a verifier derived from multi-step DPO [24]. Specifically, we begin with a base VLM  $V_{\phi_0}$ , capable of generating reasoning sequences, where  $\phi_0$  is known and encompasses all the parameters. Using multi-step DPO with preference data,  $\phi_0$  is further updated to  $\hat{\phi}_{\text{SDPO}}$ . Consequently, the verifier can be represented by  $V_{\phi_0}$  and  $V_{\hat{\phi}_{\text{SDPO}}}$  jointly.

### 3.3 Reasoner and Verifier Training

The training stage is divided into two parts: fine-tuning the reasoner with SFT and verifier training based on DPO (answer level and multi-step level). Correspondingly, the training dataset consists  $\mathcal{D}_{\text{SFT}}$  and  $\mathcal{D}_{\text{DPO}}$ , we will describe the details of Visual Tokens Scaling SFT and DPO training dataset construction in Section 4.

**Fine-tune the reasoner by SFT.** Suppose we have a base reasoning model  $\mathbb{R}_{\theta_0}$ .

*SFT training.* Given a Visual Token Scaling SFT training dataset  $\mathcal{D}_{\text{SFT}}$ , the supervised finetuning process refers to the learning of reasoner  $\mathbb{R}_{\theta}$  through minimizing the following cross-entropy loss

$$\hat{\theta}_{\text{SFT}} := \operatorname{argmin}_{\theta} \frac{1}{|\mathcal{D}_{\text{SFT}}|} \sum_{\tau \in \mathcal{D}_{\text{SFT}}} \frac{1}{H_{\tau} + 1} \mathcal{L}_{\text{SFT}}(\mathbb{R}_{\theta}(\tau), \tau),$$

where  $\mathcal{L}_{\text{SFT}}(\cdot, \cdot)$  is defined as

$$\mathcal{L}_{\text{SFT}}(\mathbb{R}_{\theta}(\tau), \tau) = - \sum_{h=1}^{H_{\tau}+1} \log \mathbb{R}_{\theta}(t_h^{\tau} | s_h^{\tau}) - \sum_{h=1}^{H_{\tau}} \log \mathbb{R}_{\theta}(a_h^{\tau} | t_h^{\tau}). \quad (2)$$

$\hat{\theta}_{\text{SFT}}$  then can be obtained by the iteration of gradient descent

$$\theta_{k+1} = \theta_k - \alpha \frac{1}{|\mathcal{D}_{\text{SFT}}|} \sum_{\tau \in \mathcal{D}_{\text{SFT}}} \frac{1}{H_{\tau} + 1} \nabla \mathcal{L}_{\text{SFT}}(\mathbb{R}_{\theta}(\tau), \tau), \quad (3)$$

where  $\alpha$  is the learning rate and the initial parameter is  $\theta_0$ .

**Verifier training by DPO.** We use multi-step DPO to derive the desired verifier that aligns with human preferences, building upon a base VLM  $V_{\phi_0}$ , such as LLaVA-v1.5-7B. Suppose we are given preference pairs  $(s_1, \tau^w, \tau^l)$ , where  $\tau^w$  is preferred trajectory over unpreferred trajectory  $\tau^l$ .

The key idea of multi-step DPO is to assume that  $r^*$  belongs to a family of one-parameter functions  $\{r_{\phi}(\cdot)\}_{\phi}$ , i.e.,  $r^*(\cdot) = r_{\phi_{\text{SDPO}}}(\cdot)$  for some unknown ground truth parameter  $\phi_{\text{SDPO}}$ . Specifically, if  $r_{\phi}(\cdot)$  is defined as

$$r_{\phi}(\tau) = \eta \sum_{h=1}^{H_{\tau}+1} \log \frac{V_{\phi}(t_h | s_h)}{V_{\phi_0}(t_h | s_h)} + \eta \sum_{h=1}^{H_{\tau}} \log \frac{V_{\phi}(a_h | t_h)}{V_{\phi_0}(a_h | t_h)} + Q(s_1),$$

where  $\eta$  is a positive constant and  $Q(\cdot)$  is a fixed function that depends only on  $s_1$ , then the preference model  $V_{\phi_{\text{SDPO}}}$  will align with the verifier  $r_{\phi_{\text{SDPO}}}$  while remaining close to the original  $V_{\phi_0}$  automatically, as shown by Equation 8 and Proposition A.1.

Furthermore,  $\phi_{\text{SDPO}}$  can be determined by maximizing the expected likelihood under the Bradley-Terry model

$$\mathbb{E}_{(s_1, \tau^w, \tau^l)} [\mathbb{P}(\tau^w \succ \tau^l)], \quad (4)$$

where

$$\mathbb{P}(\tau^w \succ \tau^l) = \sigma(r^*(\tau^w) - r^*(\tau^l)). \quad (5)$$

Once  $\phi_{\text{SDPO}}$  is obtained, the verifier  $r_{\phi_{\text{SDPO}}}$  can be used to guide the reasoner in generating the reasoning procedure. The detailed training procedure is as follows.

*Multi-step DPO.* Define the empirical multi-step DPO loss  $\mathcal{L}_{\text{SDPO}}(\phi, \phi_0)$  by equation (11). Let

$$\hat{\phi}_{\text{SDPO}} = \operatorname{argmin}_{\phi} \mathcal{L}_{\text{SDPO}}(\phi, \phi_0),$$

then  $\hat{\phi}_{\text{SDPO}}$  can be obtained by the iteration of gradient descent

$$\phi_{k+1} = \phi_k - \alpha' \sum_{(s_1, \tau^w, \tau^l) \in \mathcal{D}_{\text{DPO}}} \nabla \mathcal{L}_{\text{SDPO}}(\phi, \phi_0), \quad (6)$$

where  $\alpha'$  is the learning rate and the initial parameter is  $\phi_0$ . The verifier  $r^*$  operates on some reasoning trajectory  $\tau$  could be approximated by  $r_{\hat{\phi}_{\text{SDPO}}}(\tau)$ .

### 3.4 Inference Algorithm with Practical Efficiency and Theoretical Guarantees

In this subsection, we show our algorithm during inference time and the theoretical guarantees.

Given a new test pair  $s_1 \sim \mathcal{D}$ , we use the reasoner  $R_{\hat{\theta}_{\text{SFT}}}$  for scaling the inference sequence, and we use the verifier  $V_{\hat{\phi}_{\text{SDPO}}}$  to instruct reasoner whether to continue generating the reasoning sequence. Assume a reasoning sequence  $s_h$  is generated by the reasoner  $R_{\hat{\theta}_{\text{SFT}}}$ . We determine whether  $R_{\hat{\theta}_{\text{SFT}}}$  need to generate one additional reasoning step

$$\begin{aligned} t_h &\sim R_{\hat{\theta}_{\text{SFT}}}(\cdot | s_h), \quad a_h \sim R_{\hat{\theta}_{\text{SFT}}}(\cdot | t_h), \quad o_h = f_{a_h}(t_h), \\ s_{h+1} &= (s_h, t_h, a_h, o_h), \end{aligned} \quad (7)$$

by checking whether  $|r_{\hat{\phi}_{\text{SDPO}}}(s_{h+1}) - r_{\hat{\phi}_{\text{SDPO}}}(s_h)| \geq \epsilon$ , where  $\epsilon$  is some predetermined positive threshold. We repeat such procedure unless  $|r_{\hat{\phi}_{\text{SDPO}}}(s_{h+1}) - r_{\hat{\phi}_{\text{SDPO}}}(s_h)| < \epsilon$ . The following lemma gives an equivalent explicit termination condition.

**Lemma 3.1.** *The reasoner  $R_{\theta_0}$  stops at the reasoning step  $h$  if*

$$|r_{\hat{\phi}_{\text{SDPO}}}(s_{h+1}) - r_{\hat{\phi}_{\text{SDPO}}}(s_h)| < \epsilon \Leftrightarrow \left| \log \frac{V_{\hat{\phi}_{\text{SDPO}}}(t_h | s_h)}{V_{\phi_0}(t_h | s_h)} + \log \frac{V_{\hat{\phi}_{\text{SDPO}}}(a_h | t_h)}{V_{\phi_0}(a_h | t_h)} \right| < \epsilon.$$

Algorithm 1 characterizes the full training and test procedure of our method.

Given  $s_1 \sim \mathcal{D}$ , denote by  $H_{\tau}(\hat{\phi}_{\text{SDPO}}, \phi_0; \hat{\theta}_{\text{SFT}})^2$  the total reasoning step given by Algorithm 1, the next theorem shows that  $H_{\tau}(\hat{\phi}_{\text{SDPO}}, \phi_0; \hat{\theta}_{\text{SFT}})$  is finite almost surely (a.s.).

**Theorem 3.2** (Reasoning steps characterization). *The total reasoning step satisfies that*

1.  $H_{\tau}(\hat{\phi}_{\text{SDPO}}, \phi_0; \hat{\theta}_{\text{SFT}})$  is a stopping time.
2. (Informal). Under some mild condition,  $H_{\tau}(\hat{\phi}_{\text{SDPO}}, \phi_0; \hat{\theta}_{\text{SFT}})$  is finite with probability 1.

Theorem 3.2 shows that our algorithm is not only flexible—allowing variational reasoning steps that improve upon the results of [24]—but also guarantees a bounded number of reasoning steps. This ensures that our method avoids scenarios in which the reasoner would otherwise produce looping or repetitive outputs. The detailed proof can be found in Appendix A.4. The superiority of our algorithm can be shown in the following experiments.

## 4 Visual Tokens Scaling Dataset Construction

As discussed in Section 3, our goal is to train a *reasoner* capable of performing visual token scaling—namely, learning to invoke visual understanding tools throughout the reasoning process to generate intermediate images

<sup>2</sup>For notation simplicity, here we omit the dependence on  $s_1$ .

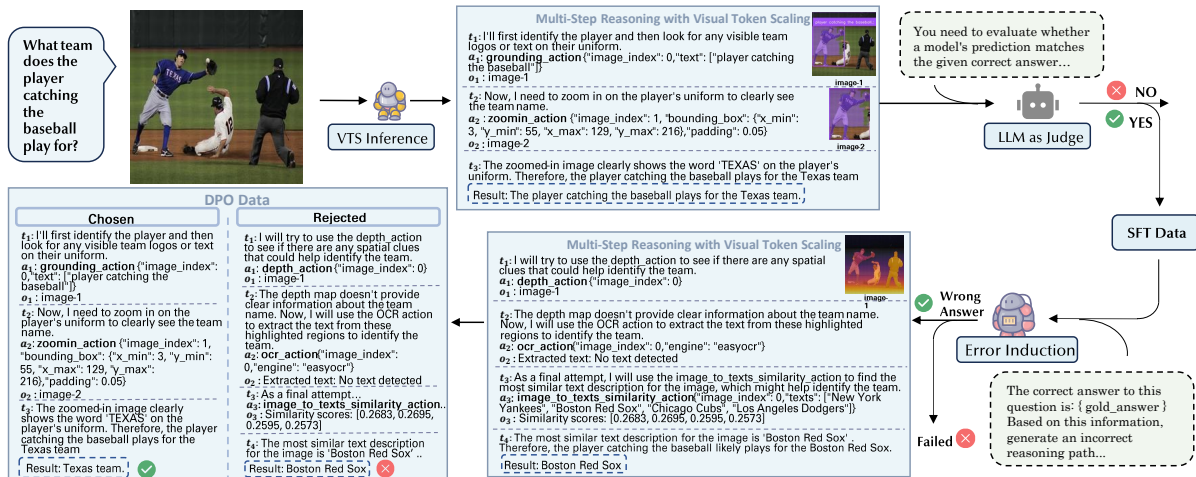


Figure 2: **Pipeline for Synthetic Data Generation and Curation in VTS-V.** Our data construction process consists of three stages: (1) generating multi-step reasoning trajectories with visual tool calls, (2) filtering out incorrect trajectories using an LLM-as-a-judge framework, and (3) creating contrastive (correct vs. incorrect) trajectory pairs for multi-step DPO training.

rich in detailed visual token information. At the same time, we aim to train a *verifier* that can distinguish between two reasoning trajectories of similar structure for the same task, identifying the one that more effectively scales visual information. This collaborative setup enables the verifier to guide and refine the reasoner’s visual reasoning process.

However, a major challenge lies in the absence of existing datasets that contain long-chain, tool-grounded reasoning traces with rich intermediate visual states. In particular, no existing datasets provide both detailed visual CoT-style supervision and curated accepted–rejected trajectory pairs required for DPO training. To address this, we construct a dedicated dataset by building upon the single-image dataset of the LLaVA-OneVision dataset (LLaVA-OV) [25], which contains 3.2M vision-language examples covering a broad range of tasks.

In this section, we describe our dataset construction pipeline in detail. Section 4.1 introduces how we collect and preprocess visual reasoning examples from LLaVA-OV to produce structured tool-based trajectories. Section 4.2 then explains how we derive both the SFT and DPO datasets from these verified trajectories.

#### 4.1 Visual Token Scaling Dataset Collection and Preprocessing

We begin our dataset construction by sampling image-question pairs from the single-image portion of the LLaVA-OV dataset, which covers a wide range of vision-language tasks such as grounding, chart understanding, OCR, and mathematical reasoning. To ensure sufficient task diversity, we uniformly sample across all 83 task types included in the dataset.

For each sampled example, we employ Qwen-2.5-VL-72B in a few-shot prompting setting to generate a visual token scaling trajectory. This trajectory is composed of a sequence of tool-based operations drawn from our predefined action space  $\mathcal{A}$  (as described in Section 3.1). In line with prior work [8, 7], the action space comprises ten visual tools: GroundingAction, DepthAction, ZoomInAction, VisualSearchAction, Crop, OCR, ImageSegment, ImageCaptioner, SimilarityComputing, and Overlay. These tools allow the model to iteratively perceive, transform, and enrich the visual content throughout the multi-step reasoning process.

Generated trajectories may include errors, invalid tool use, or inconsistent reasoning. We apply a preprocessing pipeline to flatten nested structures, merge related turns, remove malformed examples, and ensure metadata consistency. We also filter out trivial cases with no tool use and those exceeding 20,000 tokens due to memory limits. To guarantee the correctness of each trajectory, we employ the same Qwen-2.5-VL-72B model as an

LLM-based verifier (`llm_as_a_judge`) to filter out those whose final answers are deemed incorrect. Starting from over 650K generated trajectories, this process results in a curated set of 315K high-quality visual token scaling examples, which serve as the basis for supervised fine-tuning and preference training.

## 4.2 VTS-SFT and VTS-DPO Dataset Construction

Starting from the 315K verified visual token scaling trajectories described above, we construct two datasets: one for supervised fine-tuning (VTS-SFT) and one for direct preference optimization (VTS-DPO).

**VTS-SFT Dataset Construction.** To construct the VTS-SFT dataset, we transform each verified trajectory into a supervised training instance. Each trajectory  $\tau$  follows the reasoning path format defined in Equation 1, consisting of a sequence of textual states, tool actions, and visual observations, concluding with a final answer. We retain trajectories where the final answer satisfies  $t_{H_\tau+1} = t^*$ , where  $t^*$  is the ground-truth label associated with the input  $s_1$ . The resulting supervised dataset is defined as:

$$\mathcal{D}_{\text{SFT}} = \{(s_1, \tau) \mid t_{H_\tau+1} = t^*, \text{llm\_as\_a\_judge}(\tau) = \text{correct}\}.$$

Each trajectory in  $\mathcal{D}_{\text{SFT}}$  is tool-grounded and preserves all intermediate reasoning states, providing rich supervision for training. After processing, the dataset contains approximately 315K high-quality examples.

**VTS-DPO Dataset Construction.** To construct the preference dataset  $\mathcal{D}_{\text{DPO}}$ , we generate suboptimal reasoning trajectories as contrastive pairs. For each  $(s_1, \tau^w) \in \mathcal{D}_{\text{SFT}}$ , where  $\tau^w$  is a correct trajectory, we design prompts that instruct the model to begin from an intermediate point and then proceed with incorrect reasoning steps, yielding a wrong final answer, which is also the Error Induction step in Figure 2. The resulting suboptimal trajectory  $\tau^l$  is paired with  $\tau^w$  to form a preference tuple  $(s_1, \tau^w, \tau^l)$ .

We format these pairs into the standard DPO training structure and remove any example where either  $\tau^w$  or  $\tau^l$  contains empty or missing image inputs. After filtering, the final dataset  $\mathcal{D}_{\text{DPO}}$  comprises 301K preference pairs for training the verifier to assess and guide visual token scaling quality.

# 5 Experiments

We conduct comprehensive experiments to evaluate the effectiveness of our proposed Visual Token Scaling with Verification (VTS-V) framework across a range of visual reasoning tasks. This section is organized as follows: In Section 5.1, we describe the experimental setup, including model variants, training configurations, and evaluation benchmarks. Section 5.2 presents our end-to-end experiments, comparing VTS-V to several strong baselines in both closed-source and open-source settings. Finally, in Section 5.3, we conduct ablation studies to analyze the individual contributions of visual token scaling and verifier integration.

## 5.1 Experimental Setup

**Models and Baselines.** Our experiments are divided into two main parts: closed-source models and open-source models. For the closed-source setting, we follow prior work and evaluate the effectiveness of VTS-V using GPT-4o, comparing it with four strong baselines: (i) Zero-shot reasoning on GPT-4o; (ii) Chain-of-Thought (CoT) reasoning on GPT-4o; (iii) Visual prompting framework: Set-of-Mark (SoM), and Visual Sketchpad; and (iv): Tool-using framework: MMFactory.

For the open-source setting, we fine-tune three vision-language model: Qwen2-VL-7B-Instruct [26], Qwen2.5-VL-7B-Instruct[27], and LLaMA3.2-Vision-Instruct-11B on our VTS-SFT dataset. We evaluate the performance of VTS-V both before and after fine-tuning to assess its impact. Our verifier model is trained on Qwen2.5-VL-7B-Instruct using our VTS-DPO dataset. All SFT experiments are conducted using LLaMA Factory under unified settings, and DPO training is carried out with TRL. Detailed training configurations are provided in Appendix B.

**Evaluation Tasks.** We evaluate on four representative vision-language reasoning benchmarks: BLINK [1], V\*Bench [2], MMStar [28], and MathVista [29]. These benchmarks span a diverse set of capabilities, including

Model	Depth	Spatial	Jigsaw	VisCorr	SemCorr	ArtStyle	Count	FunCorr	Local	MultiV	Refl	Fore	Sim	Avg
<b>Qwen2.5-VL-7B-Instruct Variants</b>														
Qwen2.5VL-7B	65.32	83.22	56.67	40.12	24.46	58.97	65.00	19.23	41.80	43.61	25.37	34.85	79.26	49.07
Qwen2.5VL-7B + VTS-V	66.13	37.76	53.33	58.72	36.69	58.97	41.18	23.85	45.08	42.86	26.12	38.64	64.44	45.67
Ours + VTS-V	70.97	86.01	68.67	54.44	33.81	67.52	65.83	30.00	49.18	55.64	38.06	36.36	80.00	<b>56.65</b>
<b>Qwen2-VL-7B-Instruct Variants</b>														
Qwen2VL-7B	57.26	79.72	54.00	33.72	31.65	51.28	73.33	18.46	54.10	45.11	33.58	38.64	53.33	48.01
Qwen2VL-7B + VTS-V	49.19	67.83	57.05	15.72	17.56	42.74	43.33	12.90	49.59	30.83	32.84	29.55	51.85	38.54
Ours + VTS-V	60.48	60.48	58.00	37.21	40.58	76.92	63.33	28.35	51.64	47.37	35.82	34.09	84.21	<b>52.19</b>
<b>LLaMA-3.2-11B-Vision-Instruct Variants</b>														
LLaMA3.2-11B	63.71	67.13	53.33	50.58	39.57	47.86	55.00	32.31	62.30	48.12	31.34	25.76	46.67	47.98
LLaMA3.2-11B + VTS-V	-	-	-	-	-	-	-	-	-	-	-	-	-	-
Ours + VTS-V	68.55	69.23	57.33	38.60	47.48	55.56	56.67	35.43	58.20	52.63	33.58	23.48	57.46	<b>50.32</b>
<b>GPT-4o Variants</b>														
GPT-4o	74.19	69.23	55.33	75.00	53.96	82.91	49.17	40.77	59.84	59.40	37.31	79.55	72.59	62.25
GPT-4o + Sketchpad	83.90	81.10	70.70	80.80	58.30	77.19	66.70	42.10	65.40	45.60	33.10	79.00	84.20	66.78
GPT-4o + CoT	73.39	82.52	62.00	82.56	57.55	82.05	65.00	57.69	60.66	53.38	41.04	62.88	63.70	64.96
GPT-4o + SoM	68.55	76.22	49.33	83.72	52.52	-	43.33	47.69	59.84	56.40	-	-	63.70	60.13
GPT-4o + MMFactory	80.30	81.80	75.30	85.50	58.30	83.00	61.70	55.40	59.00	60.20	35.10	84.80	75.30	68.90
GPT-4o + VTS-V (Ours)	79.84	85.31	75.33	82.56	56.83	80.34	67.50	53.08	68.85	52.63	40.30	71.21	85.19	<b>69.15</b>

Table 1: **Model performance on BLINK subtasks.** Each column corresponds to a different visual reasoning task in the BLINK benchmark. Highlighted cells show whether using the proposed VTS-V method improves or degrades the performance compared to the base model.

multi-image perception and reasoning (BLINK), fine-grained understanding of small visual objects (V\*Bench), broad general knowledge QA (MMStar), and visual mathematical reasoning (MathVista). Following [7] and [30], we conduct our main experiments on 13 tasks from BLINK, a challenging and diverse benchmark designed to evaluate fine-grained visual reasoning. These tasks span visual and semantic correspondence, spatial understanding, multi-view reasoning, depth and reflectance estimation, counting, object localization, pattern alignment (e.g., jigsaw), art style comparison, functional and semantic matching, visual similarity, and forensic image detection.

## 5.2 End-to-End Experiments

**VTS-V improves performance of closed-source models.** On the BLINK benchmark, our verifier-guided visual token scaling (VTS-V) method brings robust and consistent improvements to GPT-4o. Specifically, the average performance increases from 62.25% to 69.15% (+6.90), outperforming all other prompting-based and tool-augmented variants. Compared with GPT-4o + MMFactory, VTS-V yields a slight but meaningful gain of +0.25. It shows larger improvements over GPT-4o + CoT (+3.30), GPT-4o + SoM (+9.02), and GPT-4o + Sketchpad (+2.37). The largest gains are observed on complex compositional tasks, such as Counting (+18.33), Functionally-Correlated (+12.91), and Visually-Correlated (+7.56), indicating that VTS-V strengthens reasoning over fine-grained and structured visual information.

**VTS-V enhances open-source models fine-tuned on our dataset.** Open-source models also benefit significantly from our framework. When these models are first fine-tuned on our VTS-SFT dataset and then evaluated using VTS-V, consistent gains are observed. For example, Qwen2VL-7B improves from 48.01% to 52.19% (+4.18), showing gains in Multi-view (+3.44), Local (+2.48), and Jigsaw (+4.08). Similarly, Qwen2.5VL-7B improves from 49.07% to 56.65% (+7.58), with boosts in Depth (+5.65), Spatial (+2.79), and Visual Correlation (+14.32). LLaMA3.2-11B, despite being a larger model, shows an improvement from 47.98% to 50.32% (+2.34), especially on tasks like Semantic Correlation (+8.89) and Functional Correlation (+3.12). These results demonstrate that VTS-V generalizes well to open-source architectures and consistently improves performance across vision reasoning categories.

**Fine-tuning on VTS-SFT datasets enhances models’ tool-using abilities.** We find that applying VTS-V directly to open-source models without supervised fine-tuning can harm performance. For instance, applying

VTS-V to Qwen2VL-7B drops performance from 48.01% to 38.54%, and LLaMA3.2-11B fails to output any valid tool-use actions. This behavior contrasts with GPT-4o, which can reliably follow verifier guidance even without additional training. These results suggest that base open-source models do not possess the necessary behavior patterns to interact properly with verifier signals or external tools. However, after supervised fine-tuning on our VTS-SFT dataset, these models not only recover but surpass their original performance. Post-finetuning, Qwen2VL-7B improves to 52.19%, Qwen2.5VL-7B rises to 56.65%, and LLaMA3.2-11B reaches 50.32%. More importantly, they now produce valid tool-use actions, indicating successful alignment with verifier guidance. This confirms that the VTS-SFT dataset is critical for enabling reliable tool interaction in open-source VLMs.

### VTS-V generalizes to diverse benchmarks.

To assess generalization, we evaluate models on V\*Bench[2], MMStar[28], and MathVista[29] (Table 2). Without fine-tuning, applying VTS-V can degrade performance—for instance, Qwen2.5VL-7B drops from 73.30 to 67.54 on VBench. After full training (VTS-SFT + VTS-V), performance improves across all models: Qwen2.5VL-7B reaches 75.13, Qwen2VL-7B recovers to 66.67, and LLaMA3.2-11B rises to 60.21. While LLaMA shows a drop on MathVista (30.10 to 18.81), we note that its original strength is skewed toward MathVista, with weaker performance on other benchmarks. Since our method improves general performance across models, this drop likely reflects LLaMA’s task bias rather than a limitation of VTS-V.

Trained Model	V*Bench	MMStar	MathVista
Qwen2.5VL-7B	73.30	55.00	22.60
Qwen2.5VL-7B + VTS-V	67.54	55.93	7.80
Qwen2.5VL-7B (Ours) + VTS-V	75.13	57.93	23.52
Qwen2VL-7B	66.49	53.93	22.42
Qwen2VL-7B + VTS-V	50.80	44.29	20.24
Qwen2VL-7B (Ours) + VTS-V	66.67	55.26	23.80
LLaMA-3.2-11B	54.45	50.57	30.10
LLaMA-3.2-11B + VTS-V	–	–	–
LLaMA-3.2-11B (Ours) + VTS-V	60.21	50.71	18.81

Table 2: **Model performance on general benchmarks.** Evaluation on V\*Bench, MMStar, and MathVista. Dashes indicate missing results.

### 5.3 Ablation Study and Discussion

We compare GPT-4o + VTS-V with a text-only chain-of-thought baseline (GPT-4o + CoT). VTS-V achieves 69.15% average accuracy, surpassing CoT’s 64.96% by +4.19 points. The gains are especially strong on tasks needing structured visual reasoning, such as Counting (+10.90), Functionally-Correlated (+10.98), and Visually-Correlated (+1.76). These results highlight that scaling visual reasoning via verifier-guided tool use is more effective than relying solely on extended textual reasoning.

**Verifier improves reasoning quality.** Ablation results in Table 3 clearly demonstrate the effectiveness of the verifier module. When the verifier is removed (“w/o verifier”), accuracy consistently drops across all models—Qwen2.5VL sees a decline from 54.44 to 47.09, Qwen2VL from 37.21 to 33.14, and Llama3.2vision from 38.60 to 36.63. This indicates that the verifier plays a crucial role in improving reasoning by filtering out suboptimal answer paths and enhancing decision quality. These improvements are even more pronounced compared to removing the whole VTS and verifier, which leads to further substantial accuracy drops.

	Qwen2.5VL	Qwen2VL	Llama3.2vision
Full	54.44	37.21	38.60
w/o verifier	47.09	33.14	36.63
w/o VTS-V	40.70	19.77	31.98

Table 3: Ablation results: accuracy drops when removing verifier or VTS-V.

## 6 Conclusions and Limitations

This paper presents a new framework, Visual Token Scaling with Verification (VTS-V), to enhance multi-step visual reasoning by iteratively selecting visual actions and verifying their utility at each step. By framing the process as a Markov Decision Process and integrating a verifier trained via step-wise Direct Preference

Optimization, the approach enables models to progressively refine their understanding of complex visual inputs. VTS-V achieves strong performance across a range of challenging visual reasoning benchmarks, outperforming existing baselines.

**Limitations.** The framework can be adapted to support a broader set of visual tools and more diverse reasoning formats. Enhancing the verifier’s adaptability across tasks and integrating it more tightly with downstream applications may further improve robustness. We believe VTS-V offers a flexible foundation for future research in compositional and tool-augmented visual reasoning.

## References

- [1] Xingyu Fu, Yushi Hu, Bangzheng Li, Yu Feng, Haoyu Wang, Xudong Lin, Dan Roth, Noah A Smith, Wei-Chiu Ma, and Ranjay Krishna. Blink: Multimodal large language models can see but not perceive. In *European Conference on Computer Vision*, pages 148–166. Springer, 2025.
- [2] Penghao Wu and Saining Xie. V\*: Guided visual search as a core mechanism in multimodal llms. In *Proceedings of the IEEE/CVF Conference on Computer Vision and Pattern Recognition*, pages 13084–13094, 2024.
- [3] Shengbang Tong, Zhuang Liu, Yuexiang Zhai, Yi Ma, Yann LeCun, and Saining Xie. Eyes wide shut? exploring the visual shortcomings of multimodal llms. In *Proceedings of the IEEE/CVF Conference on Computer Vision and Pattern Recognition*, pages 9568–9578, 2024.
- [4] Jarvis Guo, Tuney Zheng, Yuelin Bai, Bo Li, Yubo Wang, King Zhu, Yizhi Li, Graham Neubig, Wenhui Chen, and Xiang Yue. Mammoth-vl: Eliciting multimodal reasoning with instruction tuning at scale. *arXiv preprint arXiv:2412.05237*, 2024.
- [5] Hao Shao, Shengju Qian, Han Xiao, Guanglu Song, Zhuofan Zong, Letian Wang, Yu Liu, and Hongsheng Li. Visual cot: Unleashing chain-of-thought reasoning in multi-modal language models. *arXiv preprint arXiv:2403.16999*, 2024.
- [6] Keqin Chen, Zhao Zhang, Weili Zeng, Richong Zhang, Feng Zhu, and Rui Zhao. Shikra: Unleashing multimodal llm’s referential dialogue magic. *arXiv preprint arXiv:2306.15195*, 2023.
- [7] Yushi Hu, Otilia Stretcu, Chun-Ta Lu, Krishnamurthy Viswanathan, Kenji Hata, Enming Luo, Ranjay Krishna, and Ariel Fuxman. Visual program distillation: Distilling tools and programmatic reasoning into vision-language models. In *Proceedings of the IEEE/CVF Conference on Computer Vision and Pattern Recognition*, pages 9590–9601, 2024.
- [8] Tanmay Gupta and Aniruddha Kembhavi. Visual programming: Compositional visual reasoning without training. In *Proceedings of the IEEE/CVF Conference on Computer Vision and Pattern Recognition*, pages 14953–14962, 2023.
- [9] Dídac Surís, Sachit Menon, and Carl Vondrick. Vipergpt: Visual inference via python execution for reasoning. In *Proceedings of the IEEE/CVF International Conference on Computer Vision*, pages 11888–11898, 2023.
- [10] Jason Wei, Xuezhi Wang, Dale Schuurmans, Maarten Bosma, Fei Xia, Ed Chi, Quoc V Le, Denny Zhou, et al. Chain-of-thought prompting elicits reasoning in large language models. *Advances in neural information processing systems*, 35:24824–24837, 2022.
- [11] Jianwei Yang, Hao Zhang, Feng Li, Xueyan Zou, Chunyuan Li, and Jianfeng Gao. Set-of-mark prompting unleashes extraordinary visual grounding in gpt-4v. *arXiv preprint arXiv:2310.11441*, 2023.
- [12] Xuanyu Lei, Zonghan Yang, Xinrui Chen, Peng Li, and Yang Liu. Scaffolding coordinates to promote vision-language coordination in large multi-modal models. *arXiv preprint arXiv:2402.12058*, 2024.

- [13] Zhengyuan Yang, Linjie Li, Jianfeng Wang, Kevin Lin, Ehsan Azarnasab, Faisal Ahmed, Zicheng Liu, Ce Liu, Michael Zeng, and Lijuan Wang. Mm-react: Prompting chatgpt for multimodal reasoning and action. *arXiv preprint arXiv:2303.11381*, 2023.
- [14] Yifei Li, Zeqi Lin, Shizhuo Zhang, Qiang Fu, Bei Chen, Jian-Guang Lou, and Weizhu Chen. Making language models better reasoners with step-aware verifier. In *Proceedings of the 61st Annual Meeting of the Association for Computational Linguistics (Volume 1: Long Papers)*, pages 5315–5333, 2023.
- [15] Hunter Lightman, Vineet Kosaraju, Yuri Burda, Harrison Edwards, Bowen Baker, Teddy Lee, Jan Leike, John Schulman, Ilya Sutskever, and Karl Cobbe. Let’s verify step by step. In *The Twelfth International Conference on Learning Representations*.
- [16] Xinyu Zhu, Junjie Wang, Lin Zhang, Yuxiang Zhang, Yongfeng Huang, Ruyi Gan, Jiaying Zhang, and Yujiu Yang. Solving math word problems via cooperative reasoning induced language models. In *Proceedings of the 61st Annual Meeting of the Association for Computational Linguistics (Volume 1: Long Papers)*, pages 4471–4485, 2023.
- [17] Qianli Ma, Haotian Zhou, Tingkai Liu, Jianbo Yuan, Pengfei Liu, Yang You, and Hongxia Yang. Let’s reward step by step: Step-level reward model as the navigators for reasoning. *arXiv preprint arXiv:2310.10080*, 2023.
- [18] Peiyi Wang, Lei Li, Zhihong Shao, RX Xu, Damai Dai, Yifei Li, Deli Chen, Y Wu, and Zhifang Sui. Math-shepherd: A label-free step-by-step verifier for llms in mathematical reasoning. *arXiv preprint arXiv:2312.08935*, 2023.
- [19] Daniel M Ziegler, Nisan Stiennon, Jeffrey Wu, Tom B Brown, Alec Radford, Dario Amodei, Paul Christiano, and Geoffrey Irving. Fine-tuning language models from human preferences. *arXiv preprint arXiv:1909.08593*, 2019.
- [20] Kevin Yang, Dan Klein, Asli Celikyilmaz, Nanyun Peng, and Yuandong Tian. Rlcd: Reinforcement learning from contrastive distillation for lm alignment. In *The Twelfth International Conference on Learning Representations*.
- [21] Tomasz Korbak, Kejian Shi, Angelica Chen, Rasika Vinayak Bhalerao, Christopher Buckley, Jason Phang, Samuel R Bowman, and Ethan Perez. Pretraining language models with human preferences. In *International Conference on Machine Learning*, pages 17506–17533. PMLR, 2023.
- [22] Yixin Liu, Avi Singh, C Daniel Freeman, John D Co-Reyes, and Peter J Liu. Improving large language model fine-tuning for solving math problems. *arXiv preprint arXiv:2310.10047*, 2023.
- [23] Arian Hosseini, Xingdi Yuan, Nikolay Malkin, Aaron Courville, Alessandro Sordani, and Rishabh Agarwal. V-star: Training verifiers for self-taught reasoners. *arXiv preprint arXiv:2402.06457*, 2024.
- [24] Wei Xiong, Chengshuai Shi, Jiaming Shen, Aviv Rosenberg, Zhen Qin, Daniele Calandriello, Misha Khalman, Rishabh Joshi, Bilal Piot, Mohammad Saleh, et al. Building math agents with multi-turn iterative preference learning. *arXiv preprint arXiv:2409.02392*, 2024.
- [25] Bo Li, Yuanhan Zhang, Dong Guo, Renrui Zhang, Feng Li, Hao Zhang, Kaichen Zhang, Peiyuan Zhang, Yanwei Li, Ziwei Liu, et al. Llava-onevision: Easy visual task transfer. *arXiv preprint arXiv:2408.03326*, 2024.
- [26] Peng Wang, Shuai Bai, Sinan Tan, Shijie Wang, Zhihao Fan, Jinze Bai, Keqin Chen, Xuejing Liu, Jialin Wang, Wenbin Ge, et al. Qwen2-vl: Enhancing vision-language model’s perception of the world at any resolution. *arXiv preprint arXiv:2409.12191*, 2024.
- [27] Shuai Bai, Keqin Chen, Xuejing Liu, Jialin Wang, Wenbin Ge, Sibong Song, Kai Dang, Peng Wang, Shijie Wang, Jun Tang, et al. Qwen2. 5-vl technical report. *arXiv preprint arXiv:2502.13923*, 2025.

- [28] Lin Chen, Jinsong Li, Xiaoyi Dong, Pan Zhang, Yuhang Zang, Zehui Chen, Haodong Duan, Jiaqi Wang, Yu Qiao, Dahua Lin, et al. Are we on the right way for evaluating large vision-language models? *arXiv preprint arXiv:2403.20330*, 2024.
- [29] Pan Lu, Hritik Bansal, Tony Xia, Jiacheng Liu, Chunyuan Li, Hannaneh Hajishirzi, Hao Cheng, Kai-Wei Chang, Michel Galley, and Jianfeng Gao. Mathvista: Evaluating mathematical reasoning of foundation models in visual contexts. *arXiv preprint arXiv:2310.02255*, 2023.
- [30] Wan-Cyuan Fan, Tanzila Rahman, and Leonid Sigal. Mmfactory: A universal solution search engine for vision-language tasks. *arXiv preprint arXiv:2412.18072*, 2024.
- [31] Rafael Rafailov, Archit Sharma, Eric Mitchell, Christopher D Manning, Stefano Ermon, and Chelsea Finn. Direct preference optimization: Your language model is secretly a reward model. *Advances in Neural Information Processing Systems*, 36, 2024.
- [32] Tong Zhang. *Mathematical analysis of machine learning algorithms*. Cambridge University Press, 2023.
- [33] Rick Durrett. *Probability: theory and examples*, volume 49. Cambridge university press, 2019.

# Appendices

<b>A Proofs</b>	<b>15</b>
A.1 Verifier Obtaining . . . . .	15
A.2 Proof of Lemma 3.1 . . . . .	16
A.3 Practical Algorithm for VTS . . . . .	17
A.4 Proof of Theorem 3.2 . . . . .	17
<b>B Experimental Details</b>	<b>19</b>
<b>C Examples</b>	<b>20</b>
C.1 VTS-DPO Dataset Examples . . . . .	20
C.2 VTS-SFT Dataset Examples . . . . .	23
C.3 Benchmark Examples . . . . .	24

## A Proofs

In this section, we provide the detailed proof that is omitted in the main paper.

### A.1 Verifier Obtaining

Given the base model  $V_{\phi_0}$  and preference pairs  $(s_1, \tau^w, \tau^l)$ , the key idea of multi-step DPO ([31]; [24]) is to assume that  $r^*$  has a specific structure under which the new preference model  $V_{\phi_{\text{SDPO}}}$  and verifier  $r^*$  can be obtained by jointly solving the following KL-regularized planning problem and the maximum likelihood estimation of the Bradley-Terry model.

$$\phi_{\text{SDPO}} \in \operatorname{argmin}_{\phi} \mathbb{E}_{H_{\tau}} \mathbb{E}_{s_1 \sim \mathcal{D}, \{t_h \sim V_{\phi}(\cdot | s_h)\}_{h=1}^{H_{\tau}+1}, \{a_h \sim V_{\phi}(\cdot | t_h), o_h = f_{a_h}(t_h)\}_{h=1}^{H_{\tau}}} \left[ -r^*(\tau) + \eta \sum_{h=1}^{H_{\tau}+1} D_{\text{KL}}(V_{\phi}(\cdot | s_h) || V_{\phi_0}(\cdot | s_h)) - \eta \sum_{h=1}^{H_{\tau}} D_{\text{KL}}(V_{\phi}(\cdot | t_h) || V_{\phi_0}(\cdot | t_h)) \right], \quad (8)$$

$$\phi_{\text{SDPO}} \in \operatorname{argmin}_{\phi} -\mathbb{E}_{(s_1, \tau^w, \tau^l)} [\mathbb{P}(\tau^w \succ \tau^l)] = \operatorname{argmin}_{\phi} -\mathbb{E}_{(s_1, \tau^w, \tau^l)} [\sigma(r^*(\tau^w) - r^*(\tau^l))]. \quad (9)$$

Firstly, the next proposition shows that problem (8) can be solved directly when  $r^*$  lies in a specific family of one-parameter functions.

**Proposition A.1.** *If  $r^*(\tau) = r_{\phi'}(\tau) = \eta \sum_{h=1}^{H_{\tau}+1} \log \frac{V_{\phi'}(t_h | s_h)}{V_{\phi_0}(t_h | s_h)} + \eta \sum_{h=1}^{H_{\tau}} \log \frac{V_{\phi'}(a_h | t_h)}{V_{\phi_0}(a_h | t_h)} + Q(s_1)$  for some  $\phi'$ , where  $Q(\cdot)$  is some fixed function that only depends on  $s_1$ , then the optimal solution of problem (8) is  $\phi'$ .*

Hence if  $r^*$  takes the form  $r_{\phi'}$ , by Proposition A.1 and equation (8), we have  $r^* = r_{\phi_{\text{DPO}}}$ . Then to further obtain  $\phi_{\text{SDPO}}$ , we can plug  $r_{\phi'}(\tau)$  in equation (9) and optimize over  $\phi'$ , i.e.,

$$\begin{aligned} \phi_{\text{SDPO}} &\in \operatorname{argmin}_{\phi'} -\mathbb{E}_{(s_1, \tau^w, \tau^l)} [\sigma(r_{\phi'}^*(\tau^w) - r_{\phi'}^*(\tau^l))] \\ &= \operatorname{argmin}_{\phi'} -\mathbb{E}_{(s_1, \tau^w, \tau^l)} \left[ \log \sigma \left( \eta \left( \sum_{h=1}^{H_{\tau^w}+1} \log \frac{V_{\phi'}(t_h^{\tau^w} | s_h^{\tau^w})}{V_{\phi_0}(t_h^{\tau^w} | s_h^{\tau^w})} + \sum_{h=1}^{H_{\tau^w}} \log \frac{V_{\phi'}(a_h^{\tau^w} | t_h^{\tau^w})}{V_{\phi_0}(a_h^{\tau^w} | t_h^{\tau^w})} \right. \right. \\ &\quad \left. \left. - \sum_{h=1}^{H_{\tau^l}+1} \log \frac{V_{\phi'}(t_h^{\tau^l} | s_h^{\tau^l})}{V_{\phi_0}(t_h^{\tau^l} | s_h^{\tau^l})} - \sum_{h=1}^{H_{\tau^l}} \log \frac{V_{\phi'}(a_h^{\tau^l} | t_h^{\tau^l})}{V_{\phi_0}(a_h^{\tau^l} | t_h^{\tau^l})} \right) \right). \end{aligned} \quad (10)$$

Here we use superscript to indicate which trajectory path the reasoning steps lie in. Now we can use the following empirical multi-step DPO loss

$$\begin{aligned} \mathcal{L}_{\text{SDPO}}(\phi, \phi_0) &= - \sum_{(s_1, \tau^w, \tau^l) \in \mathcal{D}_{\text{DPO}}} \log \sigma \left( \eta \left( \sum_{h=1}^{H_{\tau^w}+1} \log \frac{V_{\phi'}(t_h^{\tau^w} | s_h^{\tau^w})}{V_{\phi_0}(t_h^{\tau^w} | s_h^{\tau^w})} + \sum_{h=1}^{H_{\tau^w}} \log \frac{V_{\phi'}(a_h^{\tau^w} | t_h^{\tau^w})}{V_{\phi_0}(a_h^{\tau^w} | t_h^{\tau^w})} \right. \right. \\ &\quad \left. \left. - \sum_{h=1}^{H_{\tau^l}+1} \log \frac{V_{\phi'}(t_h^{\tau^l} | s_h^{\tau^l})}{V_{\phi_0}(t_h^{\tau^l} | s_h^{\tau^l})} - \sum_{h=1}^{H_{\tau^l}} \log \frac{V_{\phi'}(a_h^{\tau^l} | t_h^{\tau^l})}{V_{\phi_0}(a_h^{\tau^l} | t_h^{\tau^l})} \right) \right), \end{aligned} \quad (11)$$

and obtain the optimal  $\hat{\phi}_{\text{SDPO}} \in \operatorname{argmin}_{\phi} \mathcal{L}_{\text{SDPO}}(\phi, \phi_0)$  by gradient descent. Finally, we use  $r_{\hat{\phi}_{\text{SDPO}}}$  to approximate the verifier  $r^* = r_{\phi_{\text{SDPO}}}$ .

**Proof of Proposition A.1.** The key idea is, given any  $s_1$  and  $H_{\tau}$ , using backward induction to check the optimality of  $\phi'$  for  $1 \leq h \leq H_{\tau} + 1$ . For any given  $s_h$ , define the value function  $Q_h(s_h, \phi)$  as

$$Q_h(s_h, \phi) = \mathbb{E}_{\{t_{h'} \sim V_{\phi}(\cdot | s_{h'})\}_{h'=h}^{H_{\tau}+1}, \{a_{h'} \sim V_{\phi}(\cdot | t_{h'}), o_{h'} = f_{a_{h'}}(t_{h'})\}_{h'=h}^{H_{\tau}}} \left[ -\eta \sum_{h'=h}^{H_{\tau}+1} \log \frac{V_{\phi'}(t_{h'} | s_{h'})}{V_{\phi_0}(t_{h'} | s_{h'})} \right]$$

$$\begin{aligned}
& +\eta \sum_{h'=h}^{H_\tau+1} D_{\text{KL}}(\mathbf{V}_\phi(\cdot|s_{h'})||\mathbf{V}_{\phi_0}(\cdot|s_{h'})) \\
& +\eta \mathbf{1}\{h \leq H_\tau\} \sum_{h'=h}^{H_\tau} \left( -\log \frac{\mathbf{V}_{\phi'}(a_{h'}|t_{h'})}{\mathbf{V}_{\phi_0}(a_{h'}|t_{h'})} + D_{\text{KL}}(\mathbf{V}_\phi(\cdot|t_{h'})||\mathbf{V}_{\phi_0}(\cdot|t_{h'})) \right) \Big] \\
& -\mathbf{1}\{h=1\}Q(s_1).
\end{aligned}$$

Then our goal is to show that

$$\phi' \in \operatorname{argmin}_\phi \mathbb{E}_{H_\tau} \mathbb{E}_{s_1 \sim \mathcal{D}} Q_1(s_1, \phi). \quad (12)$$

Observe that by the construction,  $Q_h(\cdot, \phi)$  satisfies the following recurrence formula

$$\begin{aligned}
& Q_h(s_h, \phi) \\
& = \mathbb{E}_{t_h \sim \mathbf{V}_\phi(\cdot|s_h), a_h \sim \mathbf{V}_\phi(\cdot|t_h), o_h = f_{a_{h+1}}(t_h)} Q_{h+1}(s_{h+1}, \phi) - \mathbf{1}\{h=1\}Q(s_1) \\
& + \eta \mathbb{E}_{t_h \sim \mathbf{V}_\phi(\cdot|s_h), a_h \sim \mathbf{V}_\phi(\cdot|t_h), o_h = f_{a_{h+1}}(t_h)} \left[ -\log \frac{\mathbf{V}_{\phi'}(t_h|s_h)}{\mathbf{V}_{\phi_0}(t_h|s_h)} + D_{\text{KL}}(\mathbf{V}_\phi(\cdot|s_h)||\mathbf{V}_{\phi_0}(\cdot|s_h)) \right] \quad (13)
\end{aligned}$$

$$+ \eta \mathbf{1}\{h \leq H_\tau\} \mathbb{E}_{t_h \sim \mathbf{V}_\phi(\cdot|s_h), a_h \sim \mathbf{V}_\phi(\cdot|t_h), o_h = f_{a_{h+1}}(t_h)} \left[ -\log \frac{\mathbf{V}_{\phi'}(a_h|t_h)}{\mathbf{V}_{\phi_0}(a_h|t_h)} + D_{\text{KL}}(\mathbf{V}_\phi(\cdot|t_h)||\mathbf{V}_{\phi_0}(\cdot|t_h)) \right]. \quad (14)$$

We now use backward induction to show that for any fixed  $s_h$ ,  $1 \leq h \leq H_\tau + 1$ ,  $\phi' \in \operatorname{argmin}_\phi Q_h(s_h, \phi)$ .

(a). For  $h = H_\tau + 1$ ,

$$Q_{H_\tau+1}(s_{H_\tau+1}, \phi) = \mathbb{E}_{t_{H_\tau+1} \sim \mathbf{V}_\phi(\cdot|s_{H_\tau+1})} \left[ -\eta \log \frac{\mathbf{V}_{\phi'}(t_{H_\tau+1}|s_{H_\tau+1})}{\mathbf{V}_{\phi_0}(t_{H_\tau+1}|s_{H_\tau+1})} + \eta D_{\text{KL}}(\mathbf{V}_\phi(\cdot|s_{H_\tau+1})||\mathbf{V}_{\phi_0}(\cdot|s_{H_\tau+1})) \right].$$

By directly using Lemma A.2, we can conclude that  $Q_{H_\tau+1}(s_{H_\tau+1}, \phi) \geq 0$ , where the equality holds when  $\mathbf{V}_\phi(\cdot|s_{H_\tau+1}) = \mathbf{V}_{\phi'}(\cdot|s_{H_\tau+1})$ . Hence  $\phi' \in \operatorname{argmin}_\phi Q_{H_\tau+1}(s_{H_\tau+1}, \phi)$ .

(b). Assume for  $h = h'$ ,  $2 \leq h' \leq H_\tau + 1$ ,  $\phi' \in \operatorname{argmin}_\phi Q_{h'}(s_{h'}, \phi)$ . Then for  $h = h' - 1$ ,

$$\phi' \in \operatorname{argmin}_\phi \mathbb{E}_{t_{h'-1} \sim \mathbf{V}_\phi(\cdot|s_{h'-1}), a_{h'-1} \sim \mathbf{V}_\phi(\cdot|t_{h'-1}), o_{h'-1} = f_{a_{h'}}(t_{h'-1})} Q_{h'}(s_{h'}, \phi).$$

To show  $\phi' \in \operatorname{argmin}_\phi Q_{h'-1}(s_{h'-1}, \phi)$ , by the definition of  $Q_{h'-1}(s_{h'-1}, \phi)$ , one only needs to show that both term (13) and term (14) obtain the minimum at  $\phi'$  when substituting  $h$  to  $h' - 1$ . This can be checked by using conditional expectation and Lemma A.2.

Hence by combining (a) and (b), we have  $\phi' \in \operatorname{argmin}_\phi Q_1(s_1, \phi)$ , which implies equation (12), as desired.  $\square$

**Lemma A.2** (Proposition 7.16 and Theorem 15.3 of [32]). *Let  $U(\cdot)$  be a given function and  $p_0(\cdot)$  be a given density function. Then the solution of*

$$\operatorname{argmin}_{p(\cdot)} \mathbb{E}_{x \sim p(\cdot)} [-U(x) + \eta D_{\text{KL}}(p(\cdot)||p_0(\cdot))]$$

is given by

$$p^*(x) = \frac{1}{C} p_0(x) \exp\left(\frac{U(x)}{\eta}\right),$$

where  $C = \log \mathbb{E}_{x \sim p_0(\cdot)} \exp\left(\frac{U(x)}{\eta}\right)$ .  $p^*(\cdot)$  is known as the Gibbs distribution.

## A.2 Proof of Lemma 3.1

*Proof of Lemma 3.1.* This is directly obtained from the definition of  $r_{\hat{\phi}_{\text{SDPO}}}$ .  $\square$

### A.3 Practical Algorithm for VTS

---

**Algorithm 1** Visual Reasoning with Visual Token Scaling and Verification

---

**Require** Training dataset  $\mathcal{D}_{\text{train}}$ , initial reasoner  $R_{\theta_0}$  and base model  $V_{\phi_0}$ .

**Input:** A new test question-image pair  $s_1 \sim \mathcal{D}$ .

**Output:** Reasoning trajectory  $\tau$ .

- 1: **Reasoning Sequence Generation:** Initialize reasoning trajectory  $\tau \leftarrow \{s_1\}$ .
  - 2: Set step counter  $h \leftarrow 1$ .
  - 3: **while** True **do**
  - 4:   **Planning:** Generate step planning  $t_h \sim R_{\hat{\theta}_{\text{SFT}}}(\cdot | s_h)$ .
  - 5:   **Action:** Select action  $a_h \sim R_{\hat{\theta}_{\text{SFT}}}(\cdot | t_h)$ .
  - 6:   **Observation:** Return  $o_h = f_{a_h}(t_h)$ .
  - 7:   Update State:  $s_{h+1} \leftarrow (s_h, t_h, a_h, o_h)$ .
  - 8:   Append  $(t_h, a_h, o_h)$  to reasoning trajectory  $\tau$ .
  - 9:   **Verification:** Compute reward difference  $\Delta r = r_{\hat{\phi}_{\text{SDPO}}}(s_{h+1}) - r_{\hat{\phi}_{\text{SDPO}}}(s_h)$ .
  - 10:   **if**  $\Delta r < \epsilon$  **then**
  - 11:     Break loop.
  - 12:   **end if**
  - 13:    $h \leftarrow h + 1$ .
  - 14: **end while**
  - 15: Generate the final result  $t_{H_\tau(\hat{\phi}_{\text{SDPO}})+1} \sim R_{\hat{\theta}_{\text{SFT}}}(\cdot | s_{H_\tau(\hat{\phi}_{\text{SDPO}})+1})$ , where  $H_\tau(\hat{\phi}_{\text{SDPO}}, \phi_0; \hat{\theta}_{\text{SFT}})$  is the total reasoning step.
  - 16: Return final trajectory  $\tau = s_{H_\tau(\hat{\phi}_{\text{SDPO}})+1} \cup \{t_{H_\tau(\hat{\phi}_{\text{SDPO}})+1}\}$ .
- 

### A.4 Proof of Theorem 3.2

Before we proceed with the main proof, we provide some relevant definitions and conclusions at the beginning.

**Definition A.3** (Martingale, supermartingale, and submartingale). Let  $\mathcal{F}_n$  be a filtration, i.e., an increasing sequence of  $\sigma$ -fields. A sequence  $X_n$  is said to be adapted to  $\mathcal{F}_n$  if  $X_n \in \mathcal{F}_n$  for all  $n$ . If  $X_n$  is a sequence with

1.  $\mathbb{E}|X_n| < \infty$ ,
2.  $X_n$  is adapted to  $\mathcal{F}_n$ ,
3.  $\mathbb{E}[X_{n+1} | \mathcal{F}_n] = X_n$  for all  $n$ ,

then  $X_n$  is said to be a martingale (with respect to  $\mathcal{F}_n$ ). If in the last definition,  $=$  is replaced by  $\leq$  or  $\geq$ , then  $X_n$  is said to be a supermartingale or submartingale, respectively.

**Definition A.4** (Stopping time). A random variable  $N$  is said to be a stopping time if  $\{N = n\} \in \mathcal{F}_n$  for all  $n < \infty$ , i.e., the decision to stop at time  $n$  must be measurable with respect to the information known at that time.

**Theorem A.5** (Martingale convergence theorem, Theorem 4.2.11 of [33]). *If  $X_n$  is a submartingale with  $\sup \mathbb{E}X_n^+ < \infty$ , then as  $n \rightarrow \infty$ ,  $X_n$  converges a.s. to a limit  $X$  with  $\mathbb{E}|X| < \infty$ .*

**Theorem A.6** (Formal version of Theorem 3.2).

1.  $H_\tau(\hat{\phi}_{\text{SDPO}}, \phi_0; \hat{\theta}_{\text{SFT}})$  is a stopping time.
2. Assume the following two conditions hold.
  - (i)  $\sup \mathbb{E}_{\tau_h \setminus \{s_1\} \sim R_{\hat{\theta}_{\text{SFT}}}(\cdot | s_1)} r_{\hat{\phi}_{\text{SDPO}}}^+(\tau_h) < \infty$  for any given  $s_1 \sim \mathcal{D}$ ,

(ii) for any  $s_{h+1}$ ,  $R_{\hat{\theta}_{\text{SFT}}}$ ,  $V_{\phi_0}$  and  $V_{\hat{\phi}_{\text{SDPO}}}$  satisfy that

$$D_{\text{KL}}\left(R_{\hat{\theta}_{\text{SFT}}}(\cdot | s_h) || V_{\phi_0}(\cdot | s_h)\right) \geq D_{\text{KL}}\left(R_{\hat{\theta}_{\text{SFT}}}(\cdot | s_h) || V_{\hat{\phi}_{\text{SDPO}}}(\cdot | s_h)\right),$$

and

$$D_{\text{KL}}\left(R_{\hat{\theta}_{\text{SFT}}}(\cdot | t_h) || V_{\phi_0}(\cdot | t_h)\right) \geq D_{\text{KL}}\left(R_{\hat{\theta}_{\text{SFT}}}(\cdot | t_h) || V_{\hat{\phi}_{\text{SDPO}}}(\cdot | t_h)\right)$$

Then  $H_\tau\left(\hat{\phi}_{\text{SDPO}}, \phi_0; \hat{\theta}_{\text{SFT}}\right)$  is finite with probability 1.

*Remark A.7 (Discussion of the conditions in Theorem A.6).* Condition (i) assumes that the verifier is finite for paths generated by reasoner  $R_{\hat{\theta}_{\text{SFT}}}$  in expectation. This can easily be achieved when the verifier is finite.

Condition (ii) can be interpreted as assuming that the distance between  $R_{\hat{\theta}_{\text{SFT}}}$  and  $V_{\phi_0}$  is greater than the distance between  $R_{\hat{\theta}_{\text{SFT}}}$  and  $V_{\hat{\phi}_{\text{SDPO}}}$ . This assumption is reasonable, as both  $R_{\hat{\theta}_{\text{SFT}}}$  and  $V_{\hat{\phi}_{\text{SDPO}}}$  align with human preferences and therefore tend to be closer to each other.

**Proof of Theorem A.6.** 1. Let  $\mathcal{F}_h$  be the smallest  $\sigma$ -field generated by  $s_{h+1}$ , i.e.,  $\mathcal{F}_h = \sigma(s_{h+1})$ . Observe that by the definition of the stopping rule as shown in equation (8),  $\left\{H_\tau\left(\hat{\phi}_{\text{SDPO}}, \phi_0; \hat{\theta}_{\text{SFT}}\right) = h\right\}$  is determined by  $s_{h+1}$ . Hence  $\left\{H_\tau\left(\hat{\phi}_{\text{SDPO}}, \phi_0; \hat{\theta}_{\text{SFT}}\right) = h\right\} \in \mathcal{F}_h$ , which implies that  $H_\tau\left(\hat{\phi}_{\text{SDPO}}, \phi_0; \hat{\theta}_{\text{SFT}}\right)$  is a stopping time.

2. By the definition of  $r_{\hat{\phi}_{\text{SDPO}}}$ , we have

$$\begin{aligned} & \mathbb{E}\left[r_{\hat{\phi}_{\text{SDPO}}}(s_{h+1}) | s_h\right] \\ &= r_{\hat{\phi}_{\text{SDPO}}}(s_h) + \mathbb{E}_{t_h \sim R_{\hat{\theta}_{\text{SFT}}}(\cdot | s_h), a_h \sim R_{\hat{\theta}_{\text{SFT}}}(\cdot | t_h), o_h = f_{a_h}(t_h)} \left[ \log \frac{V_{\hat{\phi}_{\text{SDPO}}}(t_h | s_h)}{V_{\phi_0}(t_h | s_h)} + \log \frac{V_{\hat{\phi}_{\text{SDPO}}}(a_h | t_h)}{V_{\phi_0}(a_h | t_h)} \right]. \end{aligned}$$

Observe that condition (ii) implies that

$$\begin{aligned} & \mathbb{E}_{t_h \sim R_{\hat{\theta}_{\text{SFT}}}(\cdot | s_h)} \left[ \log \frac{V_{\hat{\phi}_{\text{SDPO}}}(t_h | s_h)}{V_{\phi_0}(t_h | s_h)} \right] \\ &= D_{\text{KL}}\left(R_{\hat{\theta}_{\text{SFT}}}(\cdot | s_h) || V_{\phi_0}(\cdot | s_h)\right) - D_{\text{KL}}\left(R_{\hat{\theta}_{\text{SFT}}}(\cdot | s_h) || V_{\hat{\phi}_{\text{SDPO}}}(\cdot | s_h)\right) \\ &\geq 0, \end{aligned}$$

and

$$\begin{aligned} & \mathbb{E}_{a_h \sim R_{\hat{\theta}_{\text{SFT}}}(\cdot | t_h)} \left[ \log \frac{V_{\hat{\phi}_{\text{SDPO}}}(a_h | t_h)}{V_{\phi_0}(a_h | t_h)} \right] \\ &= \mathbb{E}_{a_h \sim R_{\hat{\theta}_{\text{SFT}}}(\cdot | t_h)} \left[ \log \frac{V_{\hat{\phi}_{\text{SDPO}}}(a_h | t_h)}{R_{\hat{\theta}_{\text{SFT}}}(a_h | t_h)} \right] + \mathbb{E}_{a_h \sim R_{\hat{\theta}_{\text{SFT}}}(\cdot | t_h)} \left[ \log \frac{R_{\hat{\theta}_{\text{SFT}}}(a_h | t_h)}{V_{\phi_0}(a_h | t_h)} \right] \\ &= D_{\text{KL}}\left(R_{\hat{\theta}_{\text{SFT}}}(\cdot | t_h) || V_{\phi_0}(\cdot | t_h)\right) - D_{\text{KL}}\left(R_{\hat{\theta}_{\text{SFT}}}(\cdot | t_h) || V_{\hat{\phi}_{\text{SDPO}}}(\cdot | t_h)\right) \\ &\geq 0, \end{aligned}$$

hence  $\mathbb{E}\left[r_{\hat{\phi}_{\text{SDPO}}}(s_{h+1}) | s_h\right] \geq r_{\hat{\phi}_{\text{SDPO}}}(s_h)$ , which indicates that  $r_{\hat{\phi}_{\text{SDPO}}}(s_h)$  is a submartingale.

Then combining condition (i) and Martingale convergence theorem A.5,  $r_{\hat{\phi}_{\text{SDPO}}}(s_h)$  converges a.s. to a limit  $\tilde{r}(s_1)$  as  $h \rightarrow \infty$ . Hence for  $\epsilon > 0$ , with probability 1, there exists a  $H_\epsilon(s_1)$  such that  $|r_{\hat{\phi}_{\text{SDPO}}}(s_{h+1}) - r_{\hat{\phi}_{\text{SDPO}}}(s_h)| < \epsilon$  when  $h > H_\epsilon(s_1)$ . Therefore,  $H_\tau\left(\hat{\phi}_{\text{SDPO}}, \phi_0; \hat{\theta}_{\text{SFT}}\right) \leq H_\epsilon(s_1)$  with probability 1, as desired.  $\square$

## B Experimental Details

Table 4: Hyperparameters for training Qwen2-VL-7B-Instruct & Qwen2.5-VL-7B-Instruct & LLaMA-3.2-11B-Vision-Instruct models

Hyperparameter	Value
LoRA Rank	8
LoRA $\alpha$	16
LoRA Dropout	0
LoRA Target	all
GPU	8 $\times$ NVIDIA A800
Per Device Train Batch Size	1
Gradient Accumulation Steps	1
Warmup Ratio	0.03
Learning Rate	3e-5
Learning Rate Scheduler	Cosine
Unfreeze Vision Tower	False
Number Train Epoch	1
Max Gradient Norm	1.0
bf16	True
Cut Off Length	65536

# C Examples

## C.1 VTS-DPO Dataset Examples

### DPO EXAMPLES

Chosen	Rejected
 <p>Q: What team hat is he wearing?</p>	 <p>Q: What team hat is he wearing?</p>
<p><b>Reasoner</b></p> <p>To determine the team hat, I will first use the <code>grounding_action</code> to locate the hat in the image. Then, I will zoom in on the hat to get a clearer view of any logos or text that might indicate the</p> <p><i>Action : <code>grounding_action</code> {"image_index": 0, "text": ["hat"]}</i></p> 	<p><b>Reasoner</b></p> <p>To determine the team hat, I'll first try to identify the logo on the cap using the <code>grounding_action</code>. This will help me recognize the team associated with the</p> <p><i>Action : <code>grounding_action</code> {"image_index": 0, "text": ["logo"]}</i></p> 
<p><b>Reasoner</b></p> <p>The hat has been located, and there seems to be a logo visible on it. I will now use the <code>zoomin_action</code> to focus on the logo for better clarity.</p> <p><i>Action : <code>zoomin_action</code> {"image_index": 2, "bounding_box": {"x_min": 171, "y_min": 182, "x_max": 272, "y_max": 260}, "padding": 0.05}</i></p> 	<p><b>Reasoner</b> <span style="color: red;">Wrong action</span></p> <p>I will now use the <span style="color: red;">visual search action</span> to thoroughly scan the image for any logos or text that could indicate the team. This will ensure I don't miss any details</p> <p><i>Action : <code>visual_search_action</code> {"image_index": 0, "objects": ["logo", "text"]}</i></p> 
<p><b>Reasoner</b></p> <p>The zoomed-in image shows a clear view of the logo on the hat. The logo appears to be 'NY', which is commonly associated with the New York Yankees baseball team. To confirm, I will use the <code>OCR</code> action to extract the text from</p> <p><i>Action : <code>ocr_action</code> {"image_index": 3, "engine": "easyocr" }</i></p>	<p><b>Reasoner</b></p> <p>The visual search action highlighted some areas but didn't clearly identify the team. I will now use the <code>OCR</code> action to extract any text from the highlighted regions to see if it reveals the team name.</p> <p><i>Action : <code>ocr_action</code> {"image_index": 2, "engine": "easyocr" }</i></p>
<p><b>Reasoner</b></p> <p>The <code>OCR</code> did not detect any text, likely due to the stylized nature of the logo. However, the visual appearance of the logo strongly resembles the 'NY' logo of the New York Yankees. Based on this observation, I can conclude that the hat is a New York Yankees hat.</p>	<p><b>Reasoner</b></p> <p>The <code>OCR</code> action did not yield clear text related to the team. Given the lack of clear identification, I will conclude that the team cannot be determined from the image.</p>
<p><b>Final Result</b></p> <p>✓ The hat is a New York Yankees hat.</p>	<p><b>Final Result</b></p> <p>✗ Unknown</p>

Figure 3: Examples of the generated DPO data.

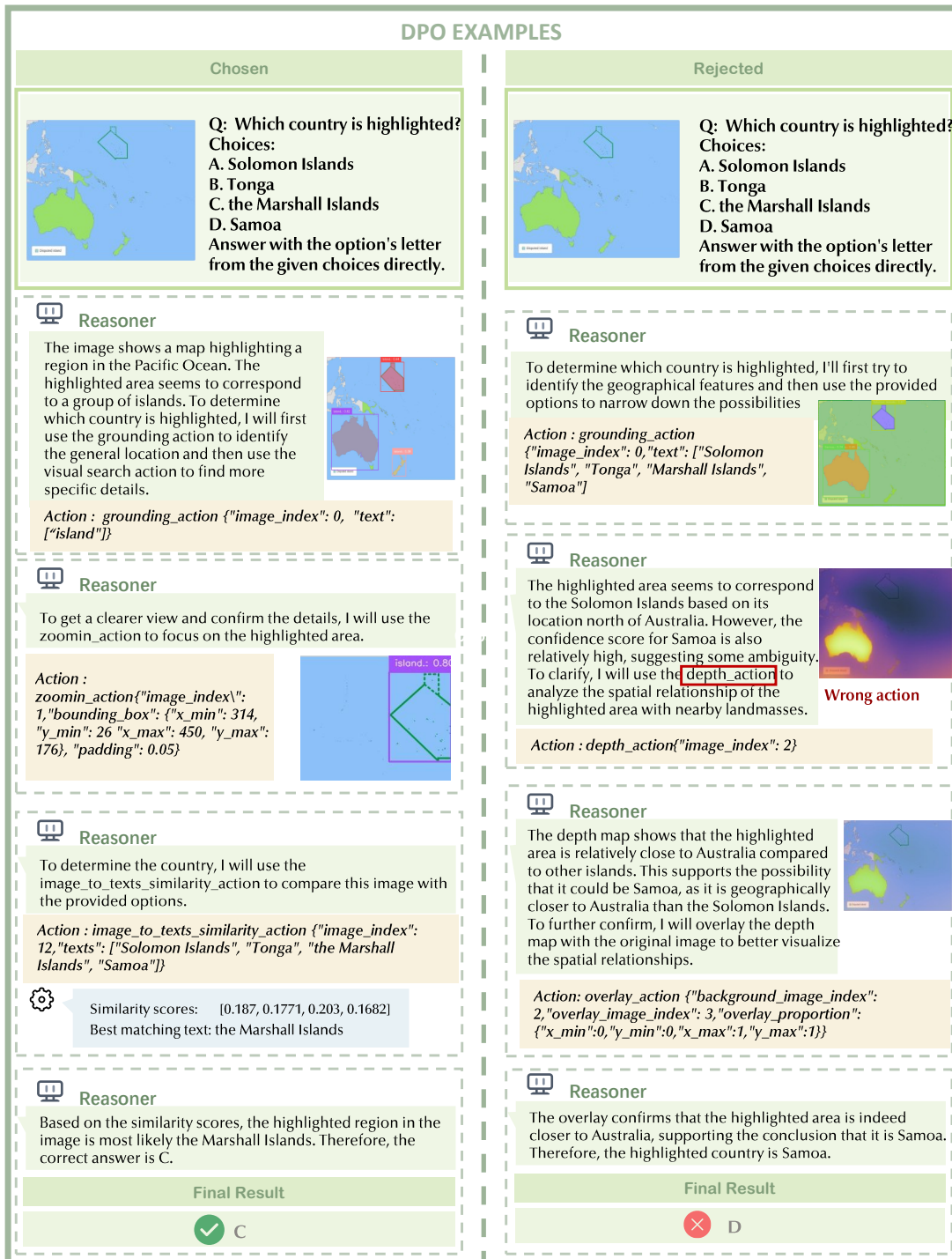


Figure 4: Additional examples of the generated DPO data.

**DPO EXAMPLES**

Chosen	Chosen
 <p style="margin-top: 10px;"><b>Q: What team does the player catching the baseball play for?</b></p>	 <p style="margin-top: 10px;"><b>Q: What team does the player catching the baseball play for?</b></p>
<p><b>Reasoner</b></p> <p>To determine which team the player catching the baseball plays for, I'll first identify the player and then look for any visible team logos or text on their uniform. I will use the grounding_action tool to locate the player catching the ball.</p>  <p style="font-family: monospace; font-size: 0.8em; background-color: #fff9c4; padding: 5px; margin-top: 10px;">Action : grounding_action {"image_index": 0, "text": ["player catching the baseball"]}</p>	<p><b>Reasoner</b> <span style="color: red; font-weight: bold;">Wrong action</span></p> <p>To determine which team the player catching the baseball plays for, I will try to use the <span style="border: 1px solid red; padding: 1px;">depth_action</span> to see if there are any spatial clues that could help identify the team. This might not directly give me the team name but could provide additional context.</p>  <p style="font-family: monospace; font-size: 0.8em; background-color: #fff9c4; padding: 5px; margin-top: 10px;">Action : depth_action {"image_index": 0}</p>
<p><b>Reasoner</b></p> <p>The player catching the baseball is highlighted. Now, I need to zoom in on the player's uniform to clearly see the team name. I will use the zoomin_action tool to focus on the player's jersey.</p>  <p style="font-family: monospace; font-size: 0.8em; background-color: #fff9c4; padding: 5px; margin-top: 10px;">Action : zoomin_action {"image_index": 1, "bounding_box": {"x_min": 3, "y_min": 55, "x_max": 129, "y_max": 216}, "padding": 0.05}</p>	<p><b>Reasoner</b></p> <p>The depth map doesn't provide clear information about the team name. Now, I will use the OCR action to extract the text from these highlighted regions to identify the team</p> <p style="font-family: monospace; font-size: 0.8em; background-color: #fff9c4; padding: 5px; margin-top: 5px;">Action : ocr_action {"image_index": 3, "engine": "easyocr"}</p> <div style="background-color: #e0e0e0; padding: 5px; font-family: monospace; font-size: 0.8em; margin-top: 5px;">       Extracted text: No text detected        Image Index: 0     </div>
<p><b>Reasoner</b></p> <p>The zoomed-in image clearly shows the word 'TEXAS' on the player's uniform. Therefore, the player catching the baseball plays for the Texas team. I will now terminate the process with the final response.</p>	<p><b>Reasoner</b></p> <p>The OCR action did not detect any text, possibly due to the angle or clarity of the image. As a final attempt, I will use the image_to_texts_similarity_action to find the most similar text description for the image, which might help identify the team.</p> <p style="font-family: monospace; font-size: 0.8em; background-color: #fff9c4; padding: 5px; margin-top: 5px;">Action : image_to_texts_similarity_action {"image_index": 0, "texts": ["New York Yankees", "Boston Red Sox", "Chicago Cubs", "Los Angeles Dodgers"]}</p> <div style="background-color: #e0e0e0; padding: 5px; font-family: monospace; font-size: 0.8em; margin-top: 5px;">       Similarity scores: [0.2683, 0.2695, 0.2595, 0.2573]        Best matching text: Boston Red Sox     </div>
<b>Final Result</b>	<b>Final Result</b>
<span style="color: green; font-size: 1.2em;">✔</span> The player catching the baseball plays for the Texas team	<span style="color: red; font-size: 1.2em;">✘</span> Boston Red Sox

Figure 5: Additional examples of the generated DPO data.

## C.2 VTS-SFT Dataset Examples

### SFT EXAMPLES



**Q:** What is the logo in the image?

**Reasoner**

To identify the logo, I will first use the OCR tool to extract any text present in the image. This will help me determine if there is a logo or brand name visible.

*Action : ocr\_action {"image\_index": 0,"engine":"easyocr"}*

Extracted text: YBE, Rs55, 8 K^rjF  
Image Index: 0

**Reasoner**

The extracted text does not seem to include a recognizable logo or brand name. Next, I will use the grounding\_action to locate any graphical elements that could represent a logo in the image.

*Action : grounding\_action {"image\_index": 0,"text": ["logo"]}*



**Reasoner**

The grounding action identified a potential logo area. Now, I will use the crop action to focus on the logo region for better clarity and further analysis.

*Action : crop\_action {"image\_index": 2,"bounding\_box": {"x\_min": 30, "y\_min": 339, "x\_max": 253, "y\_max": 562, "padding": 0.05}}*



**Reasoner**

The cropped image visually suggests a logo resembling 'Baskin Robbins'. To confirm, I will use the image\_to\_texts\_similarity\_action to compare the cropped image with text descriptions related to popular ice cream brands.

*Action : image\_to\_texts\_similarity\_action {"image\_index": 3,"texts": ["Baskin Robbins", "Ben & Jerry's", "Haagen-Dasz"]}*

Similarity scores: [0.3945, 0.2605, 0.2051]  
Best matching text: Baskin Robbins

**Reasoner**

Based on the similarity scores, the logo in the image is most likely associated with 'Baskin Robbins'.

**Final Result**

The logo in the image is Baskin Robbins.



**Q:** Given an image of an animal, identify the kind of animal in the image. The picture could be of more popular animals that are visible around zoos or are sometimes domesticated at home. They could also sometimes be found in the wild.

**Reasoner**

To identify the kind of animal in the image, I will first use the grounding\_action tool to locate any animals mentioned in the options. Since the image seems to contain elephants, I'll start by searching for 'elephant'.

*Action : grounding\_action {"image\_index": 0,"text": ["elephant"]}*



**Reasoner**

The grounding\_action tool has successfully identified several elephants in the image. Now, I will use the depth\_action tool to understand the spatial relationship of these elephants with respect to the camera and other objects in the scene.

*Action : depth\_action {"image\_index": 2}*



**Reasoner**

The depth map shows that the elephants are relatively close to the camera compared to the distant mountains. Now, I will use the overlay\_action to combine the depth map with the original image to better visualize the spatial arrangement of the elephants and their surroundings.

*Action : overlay\_action {"background\_image\_index": 2, "overlay\_image\_index": 3,"overlay\_proportion": {"x\_min": 0, "y\_min": 0, "x\_max": 1, "y\_max": 1}}*



**Reasoner**

The overlaid image confirms the presence of elephants near the water and structures. Based on the visual evidence and the successful identification of elephants in previous steps, the correct answer is clear.

**Final Result**

elephant

Figure 6: Examples of generated SFT data.

### C.3 Benchmark Examples



Figure 9: We demonstrate examples of reasoning on benchmark data using VTS-V.

## SFT EXAMPLES



**Q:** In this task, you will be provided with an image and two captions. Your task is to identify which of the two captions correctly describes the image. Options: (a) a circular sign is above a rectangular sign (b) a rectangular sign is above a circular sign

### Reasoner

To determine the correct caption, I need to analyze the arrangement of the signs in the image. The signs appear to be stacked vertically. I'll start by identifying the shapes of the signs and their order.



*Action : grounding\_action {"image\_index": 0, "text": ["circular sign", "rectangular sign"]}*

### Reasoner

The bounding boxes indicate that there is a rectangular sign positioned above a circular sign. However, there is also a triangular sign above the rectangular sign. To confirm the relationship between the rectangular and circular signs, I should focus on their positions relative to each other.

*Action : crop\_action {"image\_index": 0, "bounding\_box": {"x\_min": 730, "y\_min": 524, "x\_max": 1139, "y\_max": 754}, "padding": 0.05}*



### Reasoner

The cropped image confirms the presence of a rectangular sign with '2900 m' written on it. Now, I need to verify the position of the circular sign relative to this rectangular sign. I will proceed to crop the circular sign next.

*Action : crop\_action {"image\_index": 0, "bounding\_box": {"x\_min": 734, "y\_min": 743, "x\_max": 1142, "y\_max": 1162}, "padding": 0.05}*



### Reasoner

The cropped image confirms the presence of a circular sign with the number '70'. Based on the previous observations, the rectangular sign is indeed above the circular sign. Therefore, option (b) 'a rectangular sign is above a circular sign' is the correct description.

Final Result

Option (b) 'a rectangular sign is above a circular sign'



**Q:** Is the given caption "The couch is adjacent to the pizza." fitting for the image? Answer the question with Yes or No.

### Reasoner

To determine if the caption is fitting, I need to confirm the spatial relationship between the couch and the pizza. I will first use the grounding action to locate the couch and the pizza

*Action : grounding\_action {"image\_index": 0, "text": ["couch", "pizza"]}*



### Reasoner

The bounding boxes show that the couch and the pizza are indeed next to each other. However, to better understand the spatial arrangement, I will use the depth action to estimate the relative distances between the couch and the pizza.

*Action : depth\_action {"image\_index": 0}*



### Reasoner

The depth map indicates that the pizza is closer to the camera compared to the couch. This confirms that the couch is indeed adjacent to the pizza. Now, I will overlay the depth map with the original image to visualize the spatial relationship more clearly.

*Action : overlay\_action {"background\_image\_index": 0, "overlay\_image\_index": 3, "overlay\_proportion": {"x\_min": 0, "y\_min": 0, "x\_max": 1, "y\_max": 1}}*



### Reasoner

The overlaid image clearly shows that the couch is adjacent to the pizza. The depth map and visual confirmation support the given caption.

Final Result

Yes

Figure 7: Additional examples of generated SFT data.

### SFT EXAMPLES



**Q: Give a short and clear explanation of the subsequent image.**

**Reasoner**  
To explain the image, I will first identify the main objects present using the grounding\_action tool.

*Action: grounding\_action{"image\_index": 0, "text": ["book", "teapot", "cup"]}*



**Reasoner**  
Next, I will use the OCR tool to extract the text from the book cover to provide more details about its content.

*Action : ocr\_action {"image\_index": 2, "engine": "easyocr"}*

*Extracted text: BEST OF, Edward, THE', Abbey  
Image Index: 2*

**Reasoner**  
To further analyze the spatial arrangement of the objects, I will use the depth\_action tool to estimate the relative distances of the teapot, cup, and book from the camera.

*Action: depth\_action{"image\_index": 2}*



**Reasoner**  
Based on the depth map, the teapot, cup, and book appear to be at similar distances from the camera, lying flat on the table. Now, I will overlay the segmentation mask on the original image to better visualize the objects' boundaries.

*Action: overlay\_action {"background\_image\_index": 2, "overlay\_image\_index": 1, "overlay\_proportion": {"x\_min": 0, "y\_min": 0, "x\_max": 1, "y\_max": 1}}*



**Reasoner**  
The overlaid image clearly shows the segmentation masks for the teapot, cup, and book. All objects are well-defined and positioned on a wooden table. With all necessary information gathered, I can now provide a concise explanation of the image.

**Final Result**

The image shows a white teapot, a cup of tea with a spoon, and a book titled 'The Best of Edward Abbey' placed on a wooden table. The objects are neatly arranged, suggesting a cozy setting for reading and enjoying tea



**Q: Subtract all purple cylinders. How many purple blocks are left?**

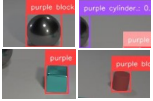
**Reasoner**  
The question asks about purple cylinders and blocks, but there are no purple objects in the image. I will first use the grounding action to confirm the absence of purple objects.

*Action : grounding\_action{"image\_index": 0, "text": ["purple cylinder", "purple block"]}*



**Reasoner**  
The grounding action did not correctly identify any purple objects. I will now use the visual search action to ensure there are no small or hidden purple objects in the image.

*Action : visual\_search\_action {"image\_index": 0, "objects": ["purple cylinder", "purple block"]}*



**Reasoner**  
The visual search action also failed to find any purple objects. I will now use the depth action to check if there are any purple objects hidden behind others.

*Action : depth\_action{"image\_index": 0}*



**Reasoner**  
The depth map shows no purple objects either. I will now use the segment action to see if there are any purple objects that were missed due to blending with the background.

*Action : segment\_action{"image\_index": 0, "bounding\_boxes": [{"x\_min": 158, "y\_min": 102, "x\_max": 236, "y\_max": 181}, {"x\_min": 345, "y\_min": 168, "x\_max": 385, "y\_max": 232}, {"x\_min": 394, "y\_min": 115, "x\_max": 436, "y\_max": 164}]}*



**Reasoner**  
The segmentation action still did not reveal any purple objects. Since all attempts to find purple objects have been unsuccessful, I can conclude that there are no purple objects in the image. Therefore, subtracting all purple cylinders would result in zero purple blocks remaining.

**Final Result**

There are 0 purple blocks left.

Figure 8: Additional examples of generated SFT data.



Figure 10: We demonstrate examples of reasoning on benchmark data using VTS-V.



Figure 11: We demonstrate examples of reasoning on benchmark data using VTS-V.